JOURNAL OF MATERIALS SCIENCE 29 (1994) 3897–3905

Texturing and texture-induced intergranular critical state anisotropy of superconducting $(Bi,Pb)_2Sr_2Ca_2Cu_3O_x$ ceramics

WAI LO, D. N. ZHENG, B. A. GLOWACKI*, A. M. CAMPBELL
IRC in Superconductivity, University of Cambridge, Madingley Road, Cambridge CB3 0HE, UK

Different techniques of texturing superconducting $(Bi,Pb)_2Sr_2Ca_2Cu_3O_x$ ceramics, including magnetic alignment, cold-die pressing, unidirectional hot pressing and a combination of these techniques, have been systematically examined with respect to the final microstructures and superconducting properties of the ceramics. The intergranular critical state of the textured ceramics was found to be anisotropic, due to a high degree of grain alignment in these materials. All the intergranular critical states in these materials could be described by the Bean model, although the temperature dependence of the average intergranular pinning force densities were different. The microstructures of the samples were characterized using scanning electron microscopy and bulk density measurement. The critical states of the textured materials were studied using a.c. magnetic susceptometry.

1. Introduction

A control of the microstructure in the polycrystalline $(Bi,Pb)_2Sr_2Ca_2Cu_3O_x$ (2223 phase) high-temperature superconductors has been repeatedly demonstrated to be essential for high bulk intergranular critical current density. Among the various microstructural parameters, the degrees of grain alignment and grain connectivity seem to be of prime importance [1–3]. The significance of fabricating grain-aligned bulk materials is that they appear to be the only materials that enable a systematic study of the intragranular properties of this compound, given that attempts to grow single-crystal samples have so far proved unsuccessful. A study of the intergranular irreversible properties using the grain-aligned materials is believed to be helpful to the understanding of the superconducting transport properties of silver-clad wires and tapes of the materials.

Several different kinds of grain-alignment techniques have been reported in the literature. These included cold and hot mechanical treatment of bulk materials and thick films [4–7], and aligning the grains at room temperature using a d.c. magnetic field [8–16]. There are advantages and disadvantages of each of the techniques, depending on the scope of applications of the techniques and the properties of the superconducting materials required. A combined use of the techniques can, therefore, possibly result in an improvement of the properties of the materials. However, the techniques have seldom been reported to have been used in conjunction with each other.

As far as the superconducting transport properties between the 2223 phase superconducting grains are concerned, a high degree of grain alignment may result in intergranular transport property anisotropy (intergranular anisotropic critical state) because the morphology of the 2223 phase grains are flake-like and the superconducting properties are anisotropic. Once it is experimentally verified, such possible texture-induced anisotropy in the intergranular superconducting transport properties will be important to the understanding of the properties of the 2223 phase tapes, which involve highly textured 2223 phase grains. It will also demand a re-formulating of the "effective medium model", which regards the coupling between the superconducting grains as a network of superconducting weak links with regular spacings and has been commonly used to explain the intergranular superconducting properties of polycrystalline bulk materials [17–19].

The present systematic study consists of two parts. The first part aims at demonstrating the limitation of each technique and the need to combine the techniques to improve the microstructures of the 2223 phase bulk materials. The techniques under study included cold pressing, magnetic alignment and hot pressing. The materials fabricated through different processes were characterized using X-ray diffractometry (XRD), scanning electron microscopy (SEM) and density measurements. The second part of the study involves a detailed investigation of the superconducting properties and the anisotropy of the inter-

* Also Department of Materials Science and Metallurgy, New Museum Site, Pembroke Street, Cambridge, CB2 3QZ, UK.

0022–2461

granular critical states of the textured materials using a.c. susceptometry (ACS).

2. Experimental procedure

2.1. Texturing of the 2223 phase ceramics

A summary of the preparation conditions of seven of the investigated samples is given in Table I. Samples 1–6 were prepared from the powders containing mostly 2223 phase, whereas Sample 7 was prepared from a precursor powder containing mainly 2212 phase instead. No additive has been employed in Sample 1. Sample 2 involved a mixture of powder and cyclohexane. Sample 3 was prepared from a suspension containing cyclohexane and a deflocculant (Hypermer KD4, ICI product). Sample 5 differs from Sample 3 by having been exposed to a 1 T d.c. magnetic field during the settling of the superconductor grains in the suspension. Samples 5 and 6 were cold pressed at different pressures, whereas no mechanical force was applied to Sample 4.

Each of the suspensions was prepared by mixing cyclohexane, KD4 and precursor powders in glass bottles, followed by vibrating the mixture for half an hour using an ultrasonic bath. To prepare Samples 4–7, the suspension was then transferred into a die located in a d.c. magnetic field, where the suspension was left to dry (Fig. 1). The dry cake thus formed was withdrawn from the magnetic field, pressed at room temperature at different pressures (except Sample 4), and the pellet shaped after pressing was removed from the die. The dispersant and any organic medium remaining in the pellet was burned off at 550 °C, a temperature determined by thermogravimetric analysis. Sintering of the bulk materials was carried out for 200 h at 830 °C, which was the optimum firing temperature for precursor materials [1].

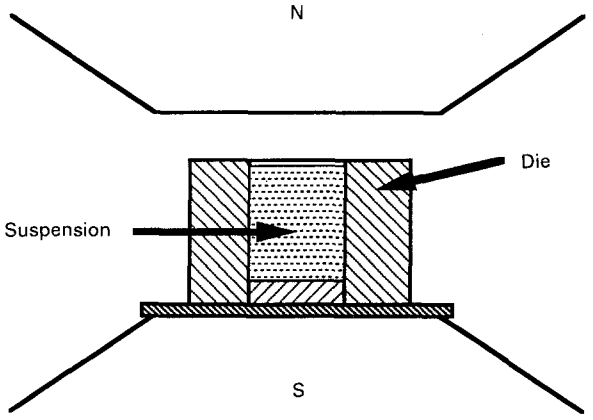

Figure 1 A schematic diagram showing the apparatus for aligning the 2223 phase grains in a suspension using a d.c. magnetic field at room temperature. N, north; S, south.

Table II summarizes the fabrication conditions of another four samples which were hot pressed. All the materials were pressed for 5 h in air and the thicknesses of the pellets before hot pressing ranged from 2–3 mm. The pressure used in each case was 5 MPa. Unlike Sample 11, which has randomly oriented 2223 phase grains before hot pressing, Samples 8–10 were prepared by hot pressing Sample 4, which had been textured by magnetic alignment, cold pressing and heat treatment. The pressing temperatures for these samples ranged from 800–830 °C.

Fig. 2 shows a schematic diagram of the apparatus used for hot pressing the samples. In carrying out the process, the material was loaded at room temperature, and was brought to the pre-determined temperature at a heating rate of 4 °C min^{-1}. It was cooled after hot pressing at a rate of 5 °C min^{-1} to room temperature, and removed from the furnace. The hot-pressed materials were then further heat treated at 830 °C for 200 h so that any displaced grains in the materials could be sintered again. Deformation and densification of the materials were estimated by comparing the dimensions and bulk densities of the materials before and after the processes.

The microstructures of the samples listed in both Tables I and II were studied by examining their fracture cross-sections and top free surfaces using scanning electron microscopy (SEM). The phases present in each sample after heat treatment were identified by powder X-ray diffractometry (XRD). The critical transition temperature of the superconducting materials were measured by a.c. magnetic susceptometry (ACS).

2.2. Intergranular critical state anisotropy of the textured 2223 phase ceramics

Fig. 3 illustrates the three kinds of critical states that may appear in well-textured materials. The direction of each critical state is defined as the direction of the gradient of the magnetic flux density. C1 is the intergranular critical state in a plane perpendicular to the lattice *c*-axis of the superconducting grains when the direction of the applied magnetic field, H_α, is parallel with the lattice *c*-axis of the grains. Because there is no microstructural anisotropy of that plane, C1 must be isotropic. When the direction of H_α is perpendicular to

TABLE I A list of the samples prepared for the study of the influences of mechanical force, magnetic field, dispersant, organic medium and starting phase composition on the microstructures of the 2223 phase bulk materials

Sample	Phases identified	Organic medium	Dispersant	Magnetic field	Pressure (MPa)
1	2223	Nil	Nil	Nil	300
2	2223	Cyclohexane	Nil	Nil	300
3	2223	Cyclohexane	KD4	Nil	300
4	2223	Cyclohexane	KD4	about 1T	0
5	2223	Cyclohexane	KD4	about 1T	300
6	2223	Cyclohexane	KD4	about 1T	900
7	2212, Ca_2PbO_4, 2201, CuO	Cyclohexane	KD4	about 1T	300

TABLE II A list of the samples prepared for the study of the influence of hot pressing on the densities and microstructure of the 2223 phase bulk materials

Sample	Source sample	Grain alignment before pressing	Load (MPa)	Temperature (°C)	Time (h)
8	5	Aligned	5	800	5
9	5	Aligned	5	815	5
10	5	Aligned	5	830	5
11	1	Randomly oriented	5	815	5

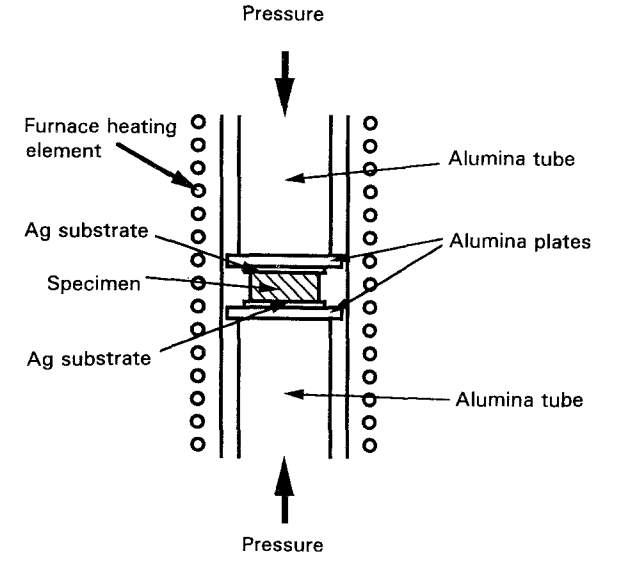

Figure 2 A schematic diagram showing the apparatus for pressing the 2223 phase pellets at high temperatures.

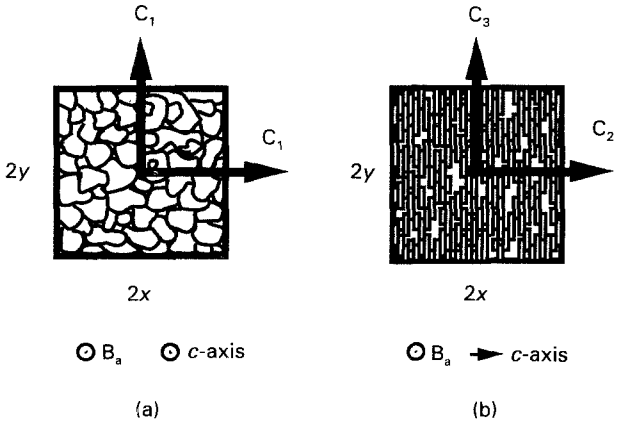

Figure 3 A diagram illustrating the three possible critical states that may exist in the textured superconducting bulk materials. H_α is the applied magnetic field. x and y are the thickness and width of the material. The critical states are denoted by C1, C2 and C3. In (a), there is no anisotropy of the weak links on the plane concerned, and C1 is therefore isotropic. Anisotropy of the critical states appear in (b), and the critical state along the c-axis is denoted C2, whereas the critical state perpendicular to the c-axis is denoted C3.

the c-axis of the grains, two different critical states in the plane perpendicular to H_α are expected to appear (C2 and C3 in Fig. 3). The critical state C2 is along the c-axis, and is created by the supercurrent flowing perpendicular to the c-axis. C3 is created by the current flowing parallel to the c-axis of the grains, and is thus perpendicular to the c-axis.

ACS has been proved to be useful in determining the average intergranular transport properties of polycrystalline superconductors [19–25]. In carrying out a measurement, the strength of the applied a.c. magnetic field is usually fixed and the magnetic susceptibility of the specimen is monitored as the temperature is changed. Because the imaginary part of the a.c. magnetic susceptibility is directly proportional to the dissipation of the superconductor in a full magnetic cycle, it usually gives a peak at a certain temperature when the magnetic flux penetrates to the centre of the specimen under measurement [19–21].

To study the intergranular critical states of the samples, it is necessary to determine the magnetic flux profiles in the specimens and the temperature dependences of the profiles. An equivalent way of achieving this is to change the specimen dimensions and find the corresponding full magnetic flux penetration field, $H_{\alpha p}$. Once the relationship between specimen dimension and $H_{\alpha p}$ is established, the models describing the critical states can be determined, and the differences between the critical states can also be distinguished.

Sample 5 has been adopted for the study of the intergranular critical states. As will be described in the following section, Sample 5 has substantial grain alignment and a low degree of grain connectivity. The transport critical current density of Sample 5 was only 100 A cm^{-2} at 77 K under zero external magnetic field [16], which then made the influence of demagnetizing factor negligible when the specimen dimensions were changed, especially near the full flux penetration states. Table III gives a summary of the characteristics of the specimens prepared from Sample 5 for the study of the intergranular critical states. The length of all the specimens was 10 mm, whereas the width and the thickness of the specimens varied, depending on the critical states the specimens were designed to illustrate (C1, C2 and C3 in Fig. 3). The purpose of preparing Samples 12–14 was to illustrate critical state C1, the critical state where the direction of the applied field, H_α, is parallel with the lattice c-axis of the superconductor grains. Samples 15–20 aimed at demonstrating C2 (the critical state along the c-axis of the grains when H_α is perpendicular to the c-axis of the grains), and Samples 21–24 were prepared for the study of C3, which is the critical state perpendicular to the c-axis when H_α is also at a right angle to the c-axis.

3. Results and discussion

3.1. Texturing of the 2223 phase bulk materials

The only phase found in the samples was the 2223 phase, and the T_c of the samples was 108 K. Fig. 4 shows a scanning electron micrograph taken from a free surface of Sample 1. As can be observed from the micrograph, the grains tend to form clusters locally, but the clusters are poorly connected, leaving a high volume of pores. Little grain alignment was noticed, except near to the free surface of the pellet. No significant difference in microstructure was found in Sample 2. Sample 3, on the other hand, showed a slight improvement in grain alignment, especially near the

TABLE III A summary of the characteristics of the grain oriented 2223 phase bulk materials used for the study of the properties of the different critical states. The critical states C1, C2 and C3 are illustated in Fig. 3. H_a is the applied magnetic field

Sample	Dimensions			Orientation of H_a	Critical state to be distinguished
	Length, l (mm)	Half width, y (mm)	Half thickness, x (mm)		
12	10	0.5	0.405	$H_a \| c$	C1
13	10	0.5	0.270	$H_a \| c$	C1
14	10	0.5	0.135	$H_a \| c$	C1
15	10	2.1	0.585	$H_a \perp c$	C2
16	10	2.1	0.360	$H_a \perp c$	C2
17	10	2.1	0.155	$H_a \perp c$	C2
18	10	2.1	0.130	$H_a \perp c$	C2
19	10	2.1	0.093	$H_a \perp c$	C2
20	10	2.1	0.075	$H_a \perp c$	C2
21	10	1.150	1.15	$H_a \perp c$	C3
22	10	0.575	1.15	$H_a \perp c$	C3
23	10	0.260	1.15	$H_a \perp c$	C3
24	10	0.100	1.15	$H_a \perp c$	C3

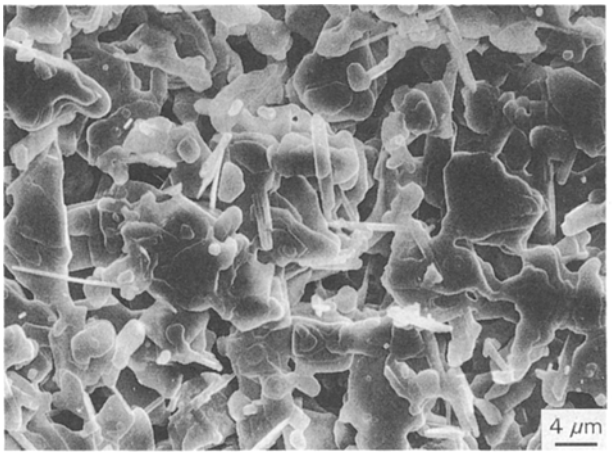

Figure 4 A scanning electron micrograph of a free surface of Sample 1, showing no global grain alignment.

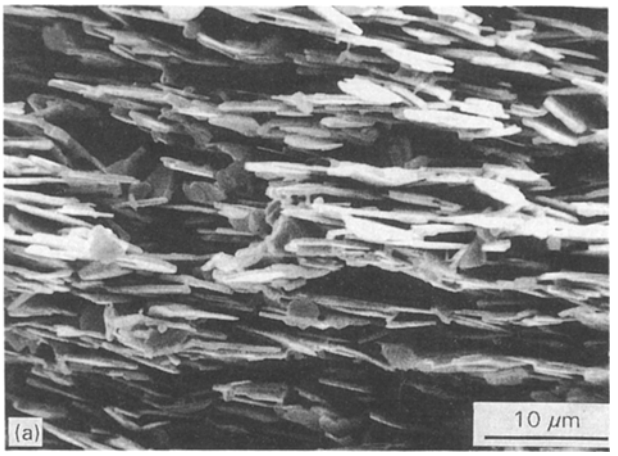

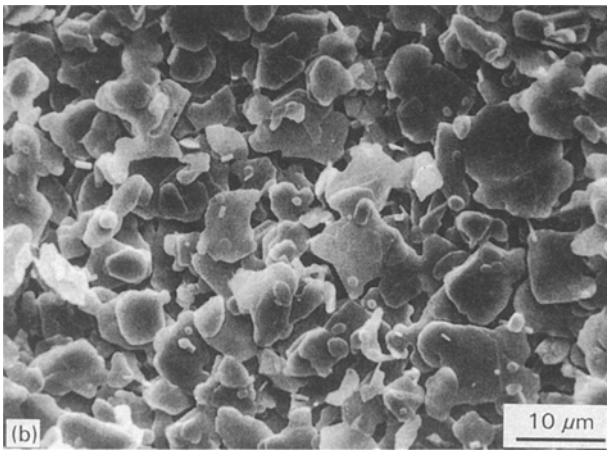

Figure 5 Scanning electron micrographs showing the microstructure of Sample 5. The micrographs were taken from the fractured cross-sections (a) along the magnetic alignment direction, and (b) perpendicular to the alignment direction.

free surface of the pellet, when compared with the microstructures of Samples 1 and 2. Furthermore, the microstructure of sample 3 was much more homogeneous. Such an improvement implies that an extensive separation of the grains in this case, as facilitated by mixing the powder with the dispersant and organic medium, is necessary if a microstructure of homogeneously well-aligned grains is needed.

Sample 4 was extremely soft and porous immediately after drying in the magnetic field, and fell into pieces when it was removed from the die. An examination of the microstructure of the pieces after heat treatment, however, showed that the grains were substantially aligned with the c-axis parallel to the direction of the magnetic field. Sample 5, which was prepared by magnetic alignment and cold pressing, provided an example of the material prepared according to the above procedure. Fig. 5 shows scanning electron micrographs of the fractured cross-sections along the alignment direction (Fig. 5a) and perpendicular to the alignment direction (Fig. 5b) of Sample 5. A high degree of grain alignment is evident from these pictures: the grains settled in the magnetic field with the lattice c-axis parallel with the magnetic field direction. The high degree of grain alignment was observed throughout the bulk of the sample, from the surface to the interior of the sample. The control of the orientation of the grains, nevertheless, is along the direction of the magnetic field only, and the magnetic field has no influence on the configuration of the grains in the perpendicular direction. As a result, the material is still

porous, and the connectivity between the grains is low (Fig. 5). On the other hand, the difference of the densities of Samples 4 and 5 suggested that mechanical force is required to shape and compact the materials after magnetic alignment.

The preparation process of Sample 6 was the same as Sample 5, except the pressure used in cold pressing after magnetic alignment was considerably higher for Sample 6 (900 MPa). This higher pressure resulted in a much denser microstructure and greater connectivity between the grains. Although Fig. 6a, which is a scanning electron micrograph of a fractured cross-section of Sample 6 in a plane parallel with the direction of the magnetic field, suggested that the density of the material might not be 100%, no voids could be identified in Fig. 6b, which is a scanning electron micrograph of a cross-section fractured perpendicular to the magnetic field direction. The arrangement of the close-packed grains is comparable with the layers of well-aligned grains near to the superconductor–silver interface in silver-clad 2223 phase tapes [2, 16, 24, 26]. Nevertheless, the sample was broken after pressing, which made direct measurement of the bulk density impossible, and prevented improvement of the properties of the material using high-pressure die pressing.

Fig. 7 shows a scanning electron micrograph of the fractured cross-section of Sample 7. The microstructure of the material shows a dense structure with locally well-aligned grains. This is due to the alignment of the grains of the 2212 phase, the predominant phase in the starting precursor. The 2212 phase grains were subsequently converted into 2223 phase grains by heat treatment. However, the degree of global alignment of the 2223 phase grains of Sample 7 is not as pronounced as in Sample 5, although the preparation conditions of both samples are exactly the same. Such a microstructural difference can be explained by the fact that the growth rate of the 2212 phase grains during its preparation is so fast that it usually distorts the texture of the materials [1], although the 2212 phase grains were well aligned before heat treatment.

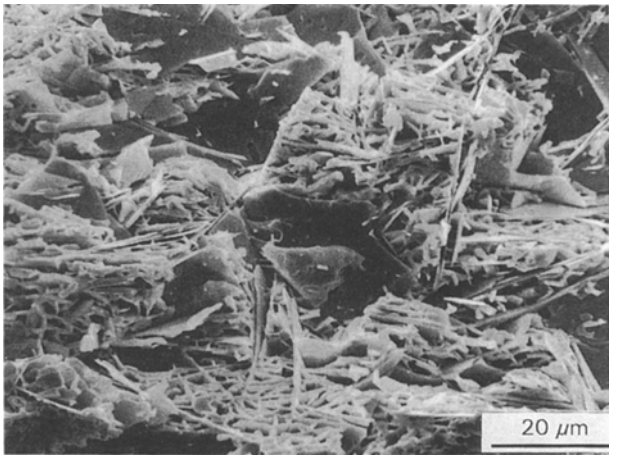

Figure 7 Scanning electron micrograph showing the microstructure of Sample 7.

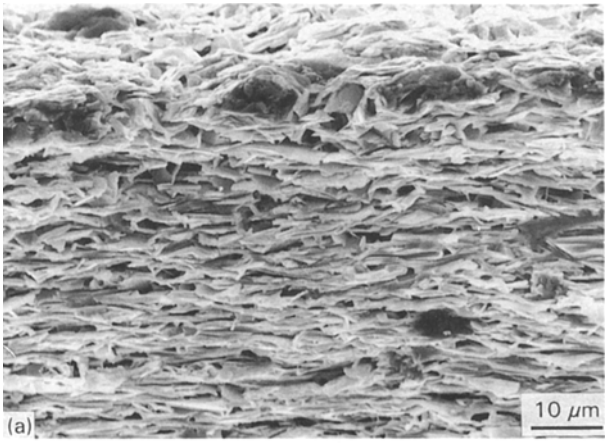

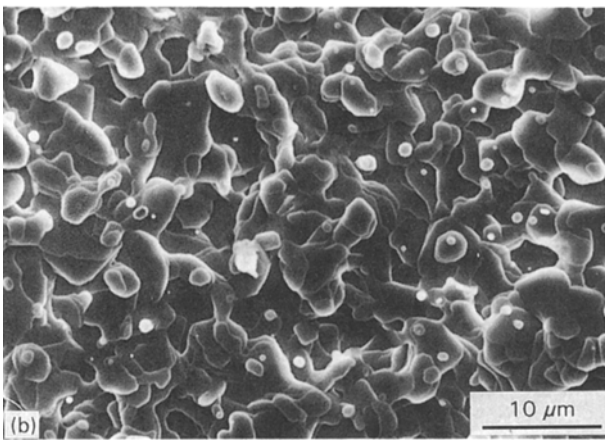

Figure 6 Scanning electron micrographs showing the microstructure of Sample 6. The micrographs were taken from the fractured cross-sections (a) along the magnetic alignment and pressing direction, and (b) perpendicular to the magnetic alignment and pressing direction.

The change in dimensions and bulk densities of the samples which were prepared by hot pressing are summarized in Table IV. The thickness of the samples was greatly reduced after the densification processes, and the substantial change in the lateral dimensions of the rectangular bars is an indication of the material migration perpendicular to the pressing direction. The influence of pressing temperature is obvious from Table IV: an increase in temperature results in more effective densification of the materials. The deformation of Sample 10, which was pressed at 830 °C, was so substantial that its dimensions, and therefore bulk density, could not be measured accurately. The choice of the appropriate pressing temperature is thus a matter of balancing the consequences of a too high deformation rate and a too low deformation rate, and according to the microstructural observations of the hot pressed materials, the appropriate temperature was chosen to be 815 °C.

After hot pressing at 815 °C, the densification of Sample 11 could be seen to have occurred. Its microstructure became compact; the grains started to have common orientation, although the degree of grain alignment was still low. Nevertheless, hot pressing is an effective way of improving the texture of materials without grain alignment.

The influence of hot pressing on materials with grain alignment was exemplified by the microstructure

TABLE IV A summary on the results of the influence of hot pressing on the densities and microstructures of the samples listed in Table II.

Sample	Before pressing			Firing temperature (°C)	After pressing		
	Grain alignment	Dimensions (mm^3)	Density ($g\ cm^{-3}$)		Grain alignment	Dimensions (mm^3)	Density ($g\ cm^{-3}$)
8	Aligned	2.73 × 15.3 × 3.0	2.30	800	Aligned	3.04 × 15.6 × 1.64	3.71
9	Aligned	2.7 × 15.3 × 2.2	2.29	815	Aligned	2.7 × 15.3 × 1.16	4.33
10	Aligned	2.7 × 15.3 × 3.0	2.29	830	–	–	–
11	Randomly orientated	3.0 × 10.0 × 2.0	2.53	815	Improved alignment	3.03 × 10.3 × 1.25	3.40

of Sample 9. A fractured cross-section of the sample, which is parallel with the direction of the magnetic field, is shown in Fig. 8a. It is clear from Fig. 8a that the grain alignment on a bulk scale has not been degraded, nor even improved, by hot pressing (as compared with Fig. 5a). However, there is still local mis-orientation of the grains, and the grains are still loosely connected. The retention of universal grain alignment and of a loose connection between the grains were further confirmed by an inspection of a fractured cross-section perpendicular to the magnetic field direction of Sample 9 (Fig. 8b). Again, grain alignment was pronounced on a large scale, but locally there are large gaps and voids between the grains. Nevertheless, although the microstructure is not as dense as in Sample 6 (Fig. 6), which has been pressed at room temperature under high pressure, the degree of connections between the grains is still higher than Sample 5 (Fig. 5), the grains of which have been magnetically aligned.

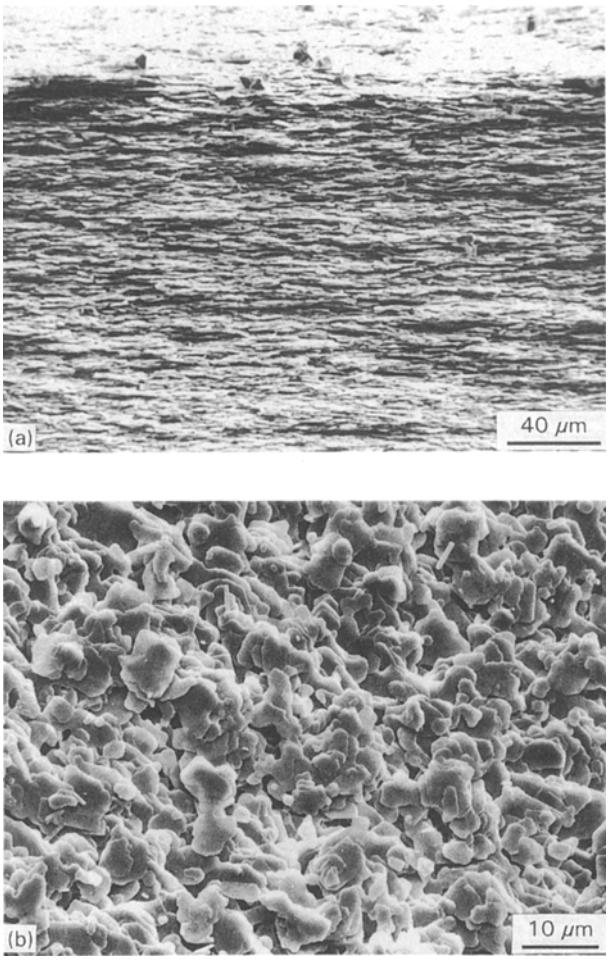

Figure 8 Scanning electron micrographs showing the microstructure of Sample 9. The micrographs were taken from the fractured cross-sections (a) along the magnetic alignment and hot-pressing direction, and (b) perpendicular to the magnetic alignment and hot-pressing direction.

3.2. Intergranular critical state anisotropy of the textured 2223 phase ceramics

Fig. 9 is a plot of the full flux penetration temperature, T_p, against the full flux penetration applied magnetic field, $H_{\alpha p}$, as extracted from the ACS results of Samples 12–14, the specimens designed to illustrate the critical state C1. A systematic reduction in T_p at constant $H_{\alpha p}$ is apparent as the thickness of the specimen is reduced, which confirms that the critical state C1 is under study.

The results of Samples 15–20 show a more complicated dependency of the depression of T_p on the specimen thickness (Fig. 10). No change of T_p for each $H_{\alpha p}$ was observed when the specimen half thickness, y, was decreased from 0.585 mm to 0.360 mm, which suggested that the critical states in these samples were not limited by C2. A change of the critical state occurred when a further reduction of y to 0.155 mm caused a significant depression of T_p. The ACS data obtained from Sample 17 was taken to be the first sign of C2 for this series of specimens. Further lowering of T_p was observed for thinner samples (Samples 18–20),

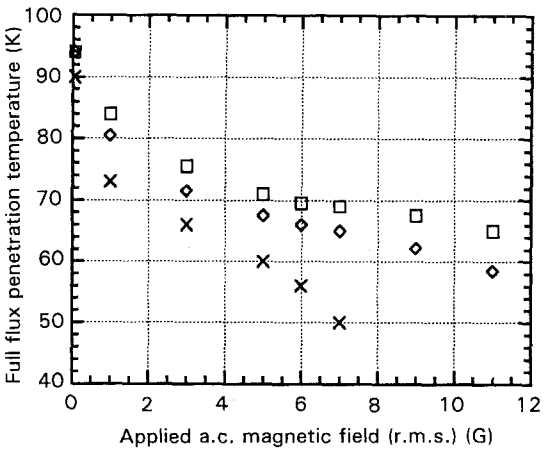

Figure 9 The dependence of the full flux penetration temperature, T_p, on the applied a.c. magnetic field for samples with different dimensions. (□) Sample 12, $x = 0.405$ mm, (◇) Sample 13, $x = 0.207$ mm, and (×) Sample 14, $x = 0.135$ mm.

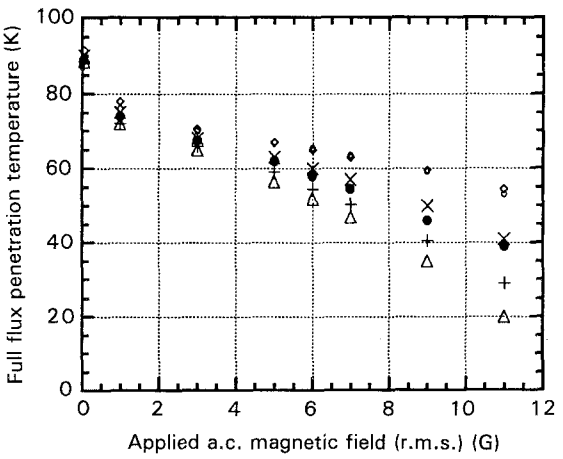

Figure 10 The dependence of the full flux penetration temperature, T_p, on the applied a.c. magnetic field for sample with different dimensions. (◇) Samples 15, $x = 0.585$ mm, (○) Sample 16, $x = 0.360$ mm, (×) Sample 17, $x = 0.155$ mm, (●) Sample 18, $x = 0.130$ mm, (+) Sample 19, $x = 0.093$ mm, and (△) Sample 20, $x = 0.075$ mm.

confirming that the critical state C2 was contributing to the ACS data.

Owing to the presence of two possible critical states, the critical state demonstrated by the results of Samples 21–24 were ambiguous in that a depression of T_p by a reduction of specimen half width, y, occurred in the first two specimens (Fig. 11). The critical states limiting specimens 21 and 22 may either be the same (because the value of $H_{\alpha p}$ depends on x) or different (specimens with different y limited by different critical states can have different $H_{\alpha p}$ at the same temperature). Nevertheless, because T_p at each $H_{\alpha p}$ was further depressed when y was further reduced, Samples 22–24 were certainly limited by C3, and any analysis of the properties of C3 will be based on the results of Samples 22–24 only.

Information on the critical state magnetic flux profiles in each set of the above specimens can be extracted from Figs. 9–11 simply by fixing a T_p in one of the figures and determine the corresponding $H_{\alpha p}$ from the sets of data belonging to samples with different specimen dimensions. The magnetic flux profile of a critical state inside a specimen can then be obtained by plotting the $H_{\alpha p}$ values against the corresponding specimen dimensions. The influence of temperature on the critical state magnetic flux profile can be found by repeating the same process with another T_p. Fig. 12 shows a plot of $H_{\alpha p}$ against half specimen thickness, x, of the critical state C1. Each set of data can clearly be fitted by a straight line, which suggests that C1 can be described by the Bean model. As can be seen from Fig. 12, the gradients of the lines are substantially diminished by an increase of temperature. The magnetic flux profiles of C2 and C3 were also found to fit the Bean model (Figs 13, 14), and the gradients of the magnetic flux profile were raised on lowering the temperatures.

A close examination of Figs 12–14 revealed that extrapolation to the zero specimen dimensions for the magnetic flux density profiles in each critical state corresponded to non-zero magnetic flux density, which is contrary to the idea of full flux penetration. The apparent contradiction can be resolved by the "effective medium model", which assumes that the microstructure of the specimens is homogeneous, and

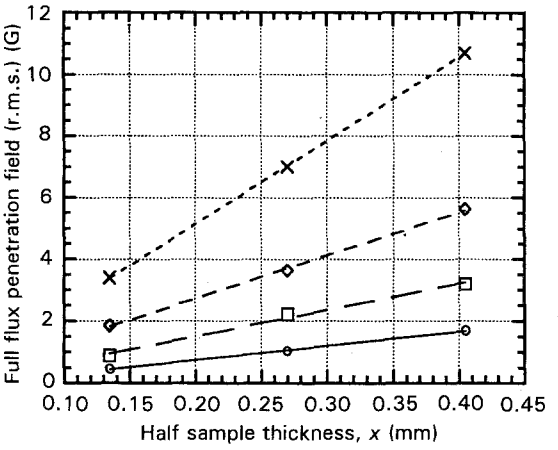

Figure 12 The relationship between the full flux penetration field and the sample dimensions at different temperatures as obtained from the data in Fig. 9: (○) at 80 K, (□) at 75 K, (◇) at 70 K, and (×) at 65 K.

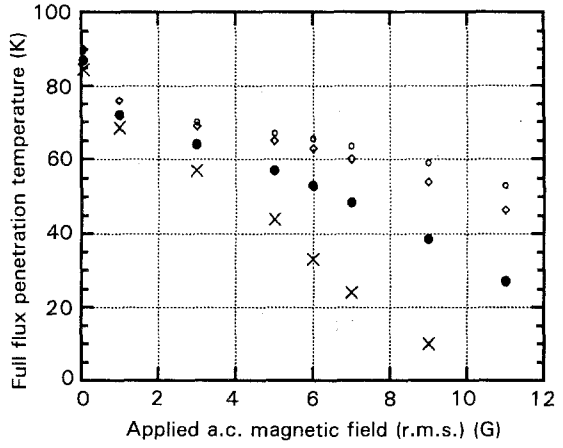

Figure 11 The dependence of the full flux penetration temperature, T_p, on the applied a.c. magnetic field for samples with different dimensions. (○) Sample 21, $y = 1.150$ mm, (◇) Sample 22, $y = 0.575$ mm, (●) Sample 23, $y = 0.260$ mm and (×) Sample 24, $y = 0.100$ mm.

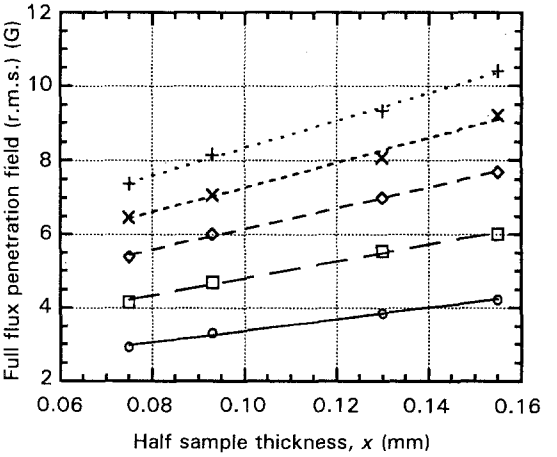

Figure 13 The relationship between the full flux penetration field and the sample dimensions at different temperatures as obtained from the data in Fig. 10: (○) at 65 K, (□) at 60 K, (◇) at 55 K, (×) at 50 K, and (+) 45 K.

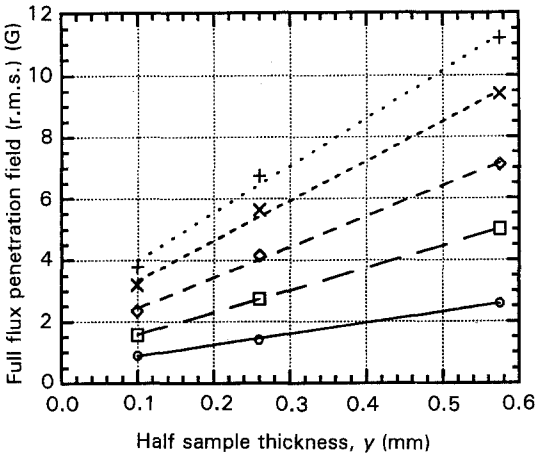

Figure 14 The relationship between the full flux penetration field and the sample dimensions at different temperature as obtained from the data in Fig. 11: (○) at 70 K, (□) at 65 K, (◇) at 60 K, (×) at 55 K, and (+) at 50 K.

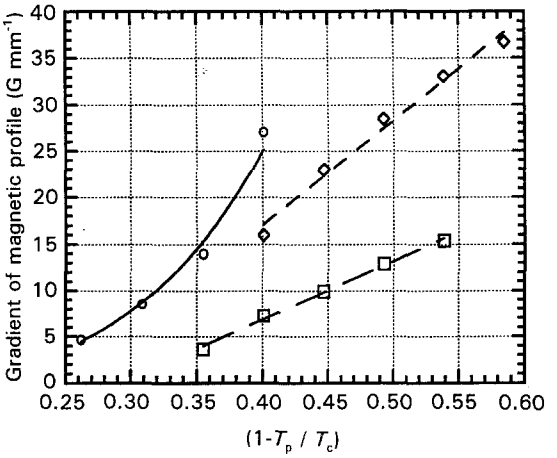

Figure 15 The relationship between the gradients of the magnetic profiles and the full flux penetration temperature of different critical states: (○) C1, data from Fig. 12, (◇) C2, data from Fig. 13, and (□) C3, data from Fig. 14.

the weak links of any possible kind were evenly distributed in the specimens. However, as the specimen dimension approaches the average dimension of the grains, the homogeneity of the material is lost, and local inhomogeneity will dominate the intergranular critical state properties of the materials. It is, therefore, inappropriate to describe the intergranular critical state properties of the small specimen dimension samples by extrapolating the properties of the homogeneous materials.

Although the gradients of the magnetic flux density profile in different critical states are all dependent on temperature, it is still possible to observe the difference of the magnetic flux density gradients of the critical states. At 65 K, for instance, the gradient of C1 (Fig. 9) is higher than those of C2 and C3 (Figs 10 and 11). The critical states of this porous, homogeneous and textured material are thus anisotropic.

To compare further the anisotropy of the critical states in the temperature domain, the gradients of each critical state magnetic flux profile in Figs 9–11 were evaluated. The results have been plotted against $(1 - T_p/T_c)$ in Fig. 15, where T_c is the superconducting critical transition temperature of the specimens. Although the temperature region in which the gradients of each critical state were obtained is slightly different, it is obvious from the figure that C1 has the steepest gradient, whereas C3 has the lowest gradient. Also presented in Fig. 15 are the best mathematical fits of the temperature dependencies of each of the critical states. The gradients of both C2 and C3 have a linear dependency on $(1 - T_p/T_c)$, whereas C1 is directly proportional to $(1 - T_p/T_c)^4$. It should be emphasized that such mathematical descriptions are only valid in the temperature regions concerned, and whether such mathematical relations will remain valid outside the temperature regions is not clear.

According to the Bean model, the gradients of the magnetic flux profiles are directly proportional to the critical current density, J_c. It can therefore be concluded that when the applied magnetic field is parallel to the lattice c-axis, the intergranular J_c, which are perpendicular to the c-axis, vary directly with $(1 - T_p/T_c)^4$. When the applied magnetic field is perpendicular to the lattice c-axis, the intergranular J_c, both perpendicular and parallel to the c-axis, are directly proportional to $(1 - T_p/T_c)$.

4. Conclusions

It is possible to align both the 2212 phase and 2223 phase superconductor grains in the precursor, which can be converted totally into the 2223 phase on heat treatment. Owing to the fast growth rate of the 2212 phase grains, the universal grain alignment in the precursor containing predominantly 2212 phase was less so after further heat treatment, although locally the grains could still reside in a common orientation. The superconductor grains needed to be dispersed in an organic suspension so that magnetic alignment, making use of the anisotropic magnetic susceptibility and flake-like morphology of the grains, was possible. Mechanical force at room temperature was essential in shaping and compacting the pellets after magnetic alignment of the grains. An increase in the mechanical force resulted in substantial densification of the material, and cracking of the material into pieces. A constant low-load and high-temperature unidirectional pressing was shown to be efficient in densifying 2223 phase bulk materials with and without grain alignment. The improvement in microstructure of the bulk material with randomly oriented grains was more substantial.

The magnetic flux profiles in the bulk 2223 phase materials with a high degree of grain alignment have been determined by examining the relationships of the full flux penetration fields and changes in the specimen dimensions. Three kinds of flux profiles, corresponding to the intergranular critical states C1, C2 and C3 described in Fig. 3, have been obtained, and all such flux profiles can be explained in terms of the Bean model. The slopes of the flux profiles, and therefore the critical current densities, of the three critical states are all different, and the flux pinning force density in C1 varies with temperature according to $(1 - T_p/T_c)^4$ whereas the flux pinning force densities in both C3

and C2 have a linear dependency on $(1 - T_p/T_c)$. The intergranular critical states of textured superconducting $(Bi,Pb)_2Sr_2Ca_2Cu_3O_x$ ceramics are therefore anisotropic.

Acknowledgements

One of the authors, Wai Lo, acknowledges the Croucher Foundation and Girton College, Cambridge for financial support.

References

1. WAI LO and B. A. GLOWACKI, in "Layered Superconductors: Fabrication, Properties and Applications", MRS Symposium Proceedings, Vol. 275, edited by D. T. Shaw, T. R. Schneider, C. C. Tsuei and Y. Shiohara (MRS, Pittsburg, PA, 1992) p. 729.
2. *Idem*, in "Advances in Cryogenic Engineering (Materials)", Vol. 38, edited by F. R. Grichett and R. P. Reed (Plenum Press, New York, 1992) p. 1065.
3. P. HALDAR, J. G. HOEHN Jr, J. A. RICE and L. R. MOTOWIDLO, *Appl. Phys. Lett.* **60** (1992) 495.
4. H. IKEDA, R. YOSHIZAKI, K. YOSHIKAWA and N. TOMITA, *Jpn J. Appl. Phys.* **29** (1990) L430.
5. N. MURAYAMA, E. SUDO, M. AWANO, K. KANI and Y. TORRI, *ibid.* **27** (1988) L1856.
6. T. UZUMAKI, K. YAMANKA, N. KAMEHARA and K. NIWA, *Appl. Phys. Lett.* **54** (1989) 2253.
7. T. ASANO, Y. TANAKA, M. FUKUTOMI, K. JIKIHARA and H. MAEDA, *Jpn J. Appl. Phys.* **4** (1989) 2253.
8. J. E. EKIN, H. R. HART Jr and A. R. GADDIPATI, *J. Appl. Phys.* **68** (1990) 2285.
9. R. H. ARENDT, A. R. GADDIPATI, M. F. GARBANSKAS, E. I. HALL, H. R. HART Jr, K. W. LAY, J. D. LIVINGTON, F. E. LUBORSKY and L. L. SCHILLING, *MRS Proc.* **99** (1991) 203.
10. R. H. ARENDT, M. F. GARBANSKAS, K. W. LAY and J. E. TKACZYK, *Phys. C.* **176** (1991) 131.
11. K. KIGIMIYA, S. KAWASHIMA, D. INOUE and S. ADACHI, *Mater. Lett.* **6** (1991) 131.
12. J. M. FERREIRA, M. B. MAPLE, H. ZHOU, R. R. HAKE, B. W. LEE, C. L. SEEMAN, M. V. KURIC and R. P. GUERTIN, *Appl. Phys. A* **47** (1988) 105.
13. B. W. STATT, Z. WANG, S. BAGHERI and J. RUTTER, *Phys. C* **183** (1991) 57.
14. S. C. PETERSON and M. J. CIMA, *J. Am. Ceram. Soc.* **71** (1988) C458.
15. T. ISHIDA, T. SAKUMA, T. SASAKI and Y. KAWADA, *Jpn J. Appl. Phys.* **28** (1989) L559.
16. B. A. GLOWACKI, WAI LO, J. YUAN, J. JACKIEWICZ and W. Y. LIANG, *IEEE Trans. Appl. Supercond.* **3** (1993) 953.
17. J. R. CLEM, *Phys. C* **153–55** (1988) 50.
18. M. TINKHAM and C. J. LOBB, in "Solid State Physics. Advances in Research and Applications", edited by H. Ehrenreich and D. Turnbull, Vol. 42 (Academic Press, London, 1989) p. 91.
19. K. H. MULLER, H. C. MacFARLANE and R. DRIVE, *Phys. C* **158** (1989) 69.
20. R. B. GOLDFARB, M. LELENTAL and C. A. THOMPSON, in "Magnetic Susceptibility of Superconductors and Other Spin Systems", edited by R. A. Hein, T. L. Francavilla and D. H. Liebenberg (Plenum Press, New York, 1991) p. 49.
21. K. H. MULLER, J. C. MacFARLANE and R. DRIVER, *Phys. C* **158** (1989) 366.
22. K. H. MULLER, *ibid.* **159** (1989) 717.
23. *Idem, ibid.* **168** (1990) 585.
24. K. H. MULLER, N. NILOLO and R. DRIVER, *Phys. Rev. B* **43** (1991) 7976.
25. S. L. SHINDE, J. MORRILL, D. GOLAND, D. A. CHANCE and T. McGUIRE, *ibid.* **41** (1990) 8838.
26. WAI LO and B. A. GLOWACKI, *Supercond. Sci. Technol.* **4** (1991) S361.
27. *Idem*, in "High Temperature Superconductors, Materials Aspects", ICMC Topical Conference Proceedings, edited by H. C. Freyhardt, R. Flukiger and M. Peuckert (Informationsgesellschaft, Verpag, 1991) p. 1005.

Received 2 February
and accepted 16 February 1994